AAPS PharmSciTech (2025) 26:56
https://doi.org/10.1208/s12249-025-03043-5

RESEARCH ARTICLE

Development of a Dermal Nanoemulsion with Antioxidants Derived from Rice Residues Using an HLD Theory Approach

Paola Vargas-Escobar[1] · Patricia Quintero-Rincón[1] · Oscar Flórez-Acosta[1]

Received: 30 August 2024 / Accepted: 8 January 2025

Abstract

Agricultural waste, such as rice straw, has become increasingly valuable as biocomposites in various industries. For cosmetic and pharmaceutical sectors, these biocomposites have improved active substance incorporation and waste reduction, which is pivotal for mitigating environmental impact. This study reports the encapsulation of a protein derivative derived from rice straw within a nanoemulsion for skin care applications, emphasizing stability and efficacy. Protein hydrolysates were produced by extracting proteins in an alkaline medium, followed by precipitation at the isoelectric point. The hydrolysates were enzymatically treated with Alcalase® at 80 °C and pH 10 for 45 min to generate antioxidant-rich formulations. Utilizing Hydrophilic-Lipophilic Deviation (HLD) theory, oil-in-water (O/W) emulsions were formulated by adjusting variables to achieve an HLD near zero. Sunflower oil and surfactants were combined, stirred at 70 °C, and homogenized using a rotor–stator. The final formulation's stability and permeability were evaluated through fluorescence microscopy, particle size analysis, zeta potential measurements, and accelerated stability assays. Nanoemulsion ENE37 showed high stability with 47.25 nm size, PDI 0.21, and excellent dispersion, maintaining integrity without phase separation. Hydrolyzed protein into ENE37 (NE37-HP) improved stability, increasing zeta potential and preventing aggregation while maintaining structure without phase inversion. NE37-HP exhibited shear-thinning behavior and good diffusion capacity, achieving 20.14 µg/cm^2.h. The HLD theory and ternary diagrams are valuable methodological tools for formulating stable nanoscale emulsions. Additionally, this dosage form, containing protein hydrolysates derived from rice straw, demonstrated potential for adequate dermal absorption in humans.

Keywords antioxidant · circular economy · HLD theory · nanoemulsion · protein hydrolysates · rice residue

Background

In recent years, industries have shifted away from non-renewable raw materials, increasingly emphasizing the use of agricultural waste to create bio-composites. Particularly in the cosmetics, pharmaceutical, and food sectors, bio-composites offer significant benefits, including incorporating active or functional substances, lending to the wastage of valuable resources, and decreasing the harmful effects of waste [1, 2].

Agriculture is a fundamental activity for human survival. It evolves by generating significant waste, for example, that generated by the rice harvest. This type of staple crop has a global production of 755.5 million tons. Although rice yields have reached more than 6100 kg ha^{-1} in America and Europe (Food and Agriculture Organization of the United Nations, 2021), the management of residual straw has become a social challenge. Residues such as straw, of which 1–1.5 kg is produced for every kilogram of rice collected during milling, and husk, which is estimated to have an equivalent production of over 200 g per kg of polished grain, are discarded into the environment, causing serious ecological problems [3, 4]. Although these residues have been used as fertilizer, animal feed, bioenergy, and biomaterial, much of it is burned, generating noxious gases and particulate matter that contribute to air pollution. This makes rice straw a problematic material if not managed properly [5].

✉ Oscar Flórez-Acosta
oscar.florez@udea.edu.co

[1] Research Group Design and Formulation of Medicines, Cosmetics, and Related, Faculty of Pharmaceutical and Food Sciences, Universidad de Antioquia, 050010 Medellin, Colombia

Published online: 04 February 2025

Straw and husk from rice contain proteins in small quantities that can serve as effective antioxidants. These proteins prevent oxidation, protect cells from free radicals and ultraviolet radiation, and mitigate skin erythema. Additionally, they stimulate collagen and elastin production, contributing to firm and flexible skin. It has recently been shown that rice residues contain insoluble polysaccharides, especially cellulose Iβ with cosmetic potential and enzymatically hydrolyzed proteins exhibit antioxidant properties, with a degree of hydrolysis of 30.41% and a 2,2-Diphenyl-1-picrylhydrazyl (DPPH) radical scavenging rate greater than 70% [6].

Studies have shown that the antioxidant effect of proteins is influenced by their composition, structure, and hydrophobicity, particularly due to specific amino acids in their sequences, including proline (Pro), methionine (Met), tryptophan (Trp), lysine (Lys), histidine (His), cysteine (Cys), and tyrosine (Tyr). Additionally, amino acids with aromatic residues enhance this antioxidant effect [7]. Proteolysis yields smaller molecules, such as protein hydrolysates and peptides, which retain the antioxidant properties of the original proteins while offering improved absorption and biological performance. However, complete proteolysis may reduce antioxidant activity, suggesting that this property arises from the synergistic interaction of various amino acids rather than from individual amino acid effects [8].

In addition to antioxidant properties, several investigations have highlighted the interfacial behavior of hydrolyzed proteins [9], that protein hydrolysates improve film strength and viscoelasticity compared to intact proteins [10]. The degree of hydrolysis affects emulsion stability, with hydrolyzed proteins displaying increased surface charge and interfacial area coverage, which improves overall emulsifying properties in various applications [11]. Gomes & Kurozawa (2023) evaluated the physicochemical properties, interfacial tension, and surface characteristics of rice protein isolate and its hydrolysates. The results showed that hydrolysis reduces the interfacial tension from 17.6 mN/m to 9.9 mN/m, even at a concentration below 1.0%. Enzymatic hydrolysis improved the protein solubility by almost 20% over a pH range of 3–11. Emulsions stabilized with rice protein hydrolysates at 1.0% concentration showed superior stability compared to emulsions stabilized with 1.5% rice protein hydrolysates, confirming the effective stabilization of the oil-in-water emulsion [12].

The growing demand for safe, eco-friendly, and sustainable products has driven researchers to explore the potential of straw and husk from rice in nanocosmetic formulations, that include nanoemulsions (NEs) [13]. NEs are nanometric emulsions that allow various active compounds to be encapsulated, providing certain advantages concerning emulsions, and that can be used for the controlled release of bioactive molecules. These lipid systems on a nanoscale are matrices characterized by semi-solid preparations at physiological temperatures, stabilized by surfactants [14]. These nanostructured encapsulation systems offer significant advantages by protecting bioactive components from oxidation, pH changes, and enzymatic degradation. They enhance solubility, bioavailability, controlled release, and targeting of encapsulated ingredients, outperforming traditional micrometer-sized carriers like macroemulsions [15].

Today, industries and consumers are more aware of the potential of natural resources and their use as raw materials to obtain new inputs [13]. Also, some studies have shown the photoprotective and anti-aging effects of antioxidant substances in skin care preparations [16, 17]. In this study, we report the encapsulation of a protein derivative extracted from rice straw into a nanoemulsion for skin care purposes. Initially, a nanoemulsion was prepared using the HLD method, with control over size and stability. Subsequently, the protein derivative was incorporated into this supporting frame, resulting in a final formulation. The preliminary evaluations that led to this formulation were based on stability, rheology, and apparent dermal permeability, informing about its potential efficacy for dermal applications.

Materials and Methods

Obtaining the Protein Hydrolysates

Protein Extraction A defatted sample of rice straw was mixed with water (1:5 ratio). The pH was adjusted to 10 with NaOH (1N) and EDTA (1 mmol) as a chelating agent to avoid proteolysis. The mixture was incubated at 40 °C for 3 h under continuous agitation and then centrifuged.

Hydrolysis Process The extracted protein (20 mg/mL) was hydrolyzed using Alcalase® (1:10 enzyme/substrate ratio) at pH 10 and 50 °C, the hydrolysis time ranged from 2.5 to 75 min. Post-hydrolysis, the enzyme was inactivated by heating the mixture at 80 °C for 15 min. The hydrolysates were then cooled, neutralized, centrifuged, and stored.

Degree of Hydrolysis (DH) DH was measured using the pH–stat method by titrating with NaOH and is expressed as the proportion of peptide bonds cleaved during hydrolysis. The antioxidant capacity of the protein hydrolysates was assessed using the DPPH free radical scavenging method. The reduction in absorbance at 517 nm after 30 min of incubation was measured to calculate the percentage of radical uptake. Results indicated a strong antioxidant activity, with the hydrolyzed protein showing a significant increase in DPPH inhibition compared to the non-hydrolyzed protein. Optimal antioxidant performance was achieved at 45 min of hydrolysis, with an inhibition percentage exceeding 70%. These

findings align with previous research by Vargas-Escobar *et al*. 2024, which demonstrated the potential of rice crop waste-derived protein hydrolysates as effective antioxidants in cosmetic applications [6].

Selection of Components and Establishment of the Formulation

Based on Eq. 1, preliminary tests were performed to achieve a stable oil-in-water (O/W) emulsion by applying HLD theory to various formulations. The objective was to obtain an O/W emulsion that theoretically develops in a slightly negative HLD region, as close to zero, to minimize interfacial forces and reduce the surfactant concentration required to produce stable microemulsions before NE formation. The resulting values allow the determination of the physicochemical equilibrium or disequilibrium, indicated by $HLD = 0$ or $HLD \neq 0$, independently of the actual values of the formulation variables. It is important to note that the same HLD value can be achieved even when formulations differ in salinity, surfactant type, temperature, and other variables. In practice, none of these variables are likely to be identical. However, they may exhibit similar physicochemical properties, allowing comparisons in terms of performance and emulsion formation [18, 19].

$$HLD = Cc - k.\,EACN - \alpha \triangle T + f(S) \quad (1)$$

where Cc is the tabulated value of the characteristic curvature of the surfactants [20], EACN is Equivalent Alkane Carbon Number (for oils and surfactants were taken from the reference value tables presented by Abbott, 2015 [20]), T is the test temperature, S is the salinity of the aqueous phase expressed in g NaCl/100 mL (this term was calculated as 0.13S for nonionic surfactants and ln (S) for ionic ones), and k, α, and f, are constants. For the EACN, k was generally taken as 0.17, while α represented the temperature difference concerning the standard state (25 °C). For anionic surfactants, $\alpha = 0.01$, and for typical ethoxylates, $\alpha = -0.06$.

For this purpose, a series of tests were developed, using sunflower oil (Sunflower oil, 100%, Sophim Peyruis, France) with an average EACN of 14. A surfactant mixture (SM), composed of Tween 80® (Polysorbate 80): Span 80® (Sorbitan Oleate), with Tween 80 being the main surfactant. Tween 80® (Soapeauty) is a water-soluble surfactant that has a Cc of −3.7, a critical micelle concentration (CMC) of 13 – 15 mg/L, a Hydrophile-Lipophile Balance (HLB): 15, cloud point of 65 °C, an experimental partition coefficient of 0.1429 and a molecular weight (MW) of 1310 g/mol; while Span 80® (Croda) is a lipophilic surfactant, which has a positive Cc of 4, an HLB of 8.6 and a MW of 428.6 g/mol [20].

Preparation Method of Nanoemulsions (NEs)

Three preliminary tests were performed using 10 test tubes to calculate the HLD values of the system, where the liposoluble phase was stained with Sudan III (Sinopharm Chemical Reagent Co., Ltd. Shanghai, China) and the aqueous phase with Methylene Blue (Ace, Johannesburg, South Africa). These tests focused on forming Winsor type III emulsion, were characterized by three distinct visible phases: an aqueous phase, an oily phase, and an intermediate phase, where the surfactant is distributed. Winsor type III emulsions are crucial in this study because they indicate areas of lower interfacial tension, where the surfactant effectively binds the oily and aqueous phases. This behavior suggests potential regions for forming more stable microemulsions or Winsor type IV nanoemulsions.

In the first test, the oil–water ratio was varied by gradually and slowly adding sunflower oil to the aqueous phase at a flow rate of approximately 0.5 mL/min (a micro drop system with a graduated chamber measured the flow rate), followed by homogenization at a rate of ramp from 3500 to 11,000 rpm (IKA T18 Basic Ultra Turrax®), S 18 D-10 G accessory), salinity (0.1 g NaCl/100 mL) and surfactant mixture (SM) concentration at 4% was kept constant, using equal proportions of Tween 80® and Span 80®. The surfactant concentration was adjusted between 0 and 10%, while the other variables remained fixed (second test). Salinity varied between 0.1 and 1.0 g NaCl/100 mL, while water, oil, and SM proportions were kept constant (third test).

Ternary System Diagram Surfactant Mix – Oil

To develop NEs with a size range of 20–200 nm and a polydispersity index (PDI) of less than 0.3, while ensuring long-term stability, another ternary phase diagram was proposed to evaluate the relationship between surfactant mix and oil, following a methodologic procedure developed in our laboratory. In this diagram, a total of 43 emulsions were assessed. HLD was calculated for each formulation, and those that did not exhibit visible separation within 48 h were subjected to measurements of particle size and PDI. Additionally, at this stage, the stability of the emulsions was determined using the Turbiscan Stability Index (TSI) with a TURBISCAN® LAB, FORMULATION (Wynnewood, PA) device. The samples were scanned at predetermined height intervals every 2 h throughout 4 to 6 days at a temperature of 40 °C to accelerate instability phenomena. This process generated light flux patterns as a function of sample height, producing transmission and backscatter (BS) profiles. The data obtained were analyzed using the Turbisoft version 1.21 software program, following the methodology outlined in Eq. 2 [20].

$$TSI = \sum_{T^{\circ}=1} \Sigma \frac{\overset{h=H}{\underset{h=0}{}} |BS_t\ (h) - BS_{t-1}(h)|}{H} \quad (2)$$

where, T° is the temperature, H and h is the height of the samples in the devices, t is the time, and BS is the backscatter.

Incorporation of Proteins and Hydrolysates in the NEs

Recent studies have demonstrated that 1.0% rice protein hydrolysates exhibit significantly low interfacial tension, which enhances solubility and stabilizes oil/water emulsions [12]. Building on this knowledge, we conducted preliminary preparations that indicated optimal stability, as well as favorable particle size and polydispersity index. Consequently, a specific formulation was selected as the supporting framework or base formula for incorporating protein derivatives obtained from extracted rice waste. These protein derivatives were integrated into the NE following the established preparation method, with a concentration of 1.0% added to the aqueous phase of the NE.

Statistical analyses and surface contour graphs were generated with the software Statgraphics® (StatPoint, Inc., The Plains, United States) and OriginLab (OriginLab Corporation, Northampton, Massachusetts, USA). These analyses enabled the visualization of HLD values for each system of variables evaluated. All tests were conducted in triplicate, and results are presented as the mean ± standard deviation. Data analysis was performed using a one-way ANOVA test, with p values < 0.05 considered significant. Additionally, the software was used to create contour graphs in the ternary diagrams.

Characterization of NEs

Verification of the Type of NEs

In an inverted fluorescence microscope equipped with phase-contrast capabilities (IN300T-FL, AMSCOPE, USA) and an Optitec YG-100 fluorescence lamp, the evaluation of staining with sodium fluorescein was conducted. This setup included a digital camera and a 40X objective lens. The spot fluorescence indicated the formation of O/W nanoemulsions, while continuous fluorescence suggested the presence of W/O nanoemulsions [21].

Dispersibility Studies

An ERWEKA 8537–060 dissolution apparatus was employed to evaluate NEs. Each glass vessel was filled with 500 mL of distilled water maintained at 37 ± 0.5 °C. Subsequently, 2.1 mL of each formulation was added using a USP type 1 apparatus set at a stirring speed of 50 rpm. The performance of the nanoemulsions was assessed visually according to the scale proposed by Gurpreet & Singh (2018) [22]: Grade A: The formulation disperses quickly within 1 min and appears transparent or bluish. Grade B: The formulation disperses quickly and appears bluish-white. Grade C: A thin milky emulsion forms within 2 min or less. Grade D: The formulation is opaque, grayish-white in color with an oily appearance, and disperses more slowly (greater than 2 min). Grade E: There is poor or negligible emulsification, characterized by large oil globules on the surface. The pH was taken directly using a pH meter HANDYLAB 1, 62,531,084, SCHOTT-Geräte GmbH, Germany.

Rheological Properties

Rheological properties were carried out in a laboratory rheometer, ANTON PAAR MCR72/92, Graz, Austria, coupled with a geometry of concentric cylinders, at a temperature of 25.0 °C ± 0.1, controlled with a temperature device, PELTIER RheolabQC PLUS, C-PTD180/AIR/QC. The experimental flow curves were made with a shear rate of 0.1 – 100 s^{-1}, and They were adjusted to the Newton, Power Law, Bingham, Herschel – Bulkley, and Casson models, calculating the consistency coefficient (K) and the flow behavior index (n). For a Newtonian emulsion n = 1 and for an emulsion that presents a shear thinning behavior n < 1. Additionally, the apparent viscosity was evaluated at a shear rate of 60 s^{-1} to compare the emulsions since the human perception of the thickness is correlated with the apparent viscosity at this shear rate [23].

Viscosity

Viscosity was calculated with Eq. 3

$$\eta = K\dot{\gamma}N^{-1} \quad (3)$$

where η is the viscosity, K is a proportionality constant, $\dot{\gamma}$ is the strain rate and N is the flow behavior index.

Amplitude Sweep

Amplitude sweep was performed in a strain range of 0.1 to 100 under a fixed frequency of 1 Hz, linear viscoelastic region (LVR), and the transition point (where G' = G'') were extracted from the graph [24].

Frequency Sweep

The analysis of frequency sweep was performed in a range of 0.01 to 100 rad/s at a fixed temperature of 25 °C and a

constant voltage of 0.1 V, determined from the amplitude sweep test. The storage modulus (G') and loss modulus (G") were measured at different frequencies, demonstrating the effect of frequency on the rheological properties of the O/W emulsions.

Measurement of Particle size (PS), Polydispersity Index (PDI), and Zeta Potential (ζ)

The PS and the PDI were determined by Dynamic Light Scattering (DLS), while for the ζ the surface charge of the particle or zeta potential was determined by measuring the electrophoretic mobility of the droplets. It is taken as a reference that a ζ of ± 30 mV was sufficient to guarantee the physical stability of the NE [22]. These three tests were carried out in a NANO-ZS 90 equipment, NANO-ZS 90, MALVERN INSTRUMENTS (Worcestershire, UK), at a wavelength of 633 nm at 90°. To avoid multiple dispersion effects, the formulations were diluted with filtered deionized water. Measurements were performed in triplicate.

Preliminary Stability Studies

Stability Prediction Using the Turbiscan Stability Index (TSI)

Stability was evaluated using multiple light scattering data, specifically through the backscatter and transmission functions. These measurements were summarized into a single value that indicates the system's destabilization. High TSI values correspond to low stability and a higher probability of phase separation [25, 26].

Accelerated Thermodynamic Stability

A series of accelerated tests were conducted to evaluate the physical stability of the final preparation and to predict its shelf life. The samples were subjected to six cycles of temperature fluctuations between 5 °C and 40 °C for a duration of 48 h. Formulations that remained stable at these temperatures were then centrifuged at 5000 rpm for 30 min. Observations indicated that these formulations did not exhibit phase separation, cream formation, or cracking of the NEs. Subsequently, the formulations that showed no signs of instability were subjected to three additional cycles with varying temperatures between 5 °C and 25 °C. Any formulation that maintained stability throughout these stages was deemed to possess good stability. Furthermore, the stability of the NEs was assessed after each cycle by measuring the PS and PDI. The stability index of the optimized NE formulation was calculated using Eq. 4, providing a quantitative measure of its stability under the tested conditions [27]:

$$\text{Stability Index NEs} = \frac{\text{PS Initial} - \text{PS Time}}{\text{PS Initial}} \quad (4)$$

Measurement of the Permeability of NEs

Based on the knowledge that the permeability of active ingredients through the skin can be improved with nanometric formulations [28, 29], transdermal transfusion and permeation were determined. In brief, transdermal diffusion was determined using the Franz cell device CENTRICOL (Medellín, Colombia) with 10 cells, each containing 10.5 mL of acetate buffer (pH 5.5) in the receiving medium and 3 mL of emulsion in the donor cells. Strat-M® membranes were used for permeation. Throughout the test, the temperature and magnetic stirring conditions of the receiving medium were maintained at 32 °C and 300 rpm, respectively. Sampling, with buffer replacement, was conducted at 1.0, 2.0, 3.0, 4.0, 5.0, and 6.0 h. The amount of protein material that crossed the membrane was quantified using Bradford reagent by Ultraviolet (UV) spectroscopy at a wavelength of 595 nm, employing a calibration curve.

Permeation calculations were obtained from a regression curve at different times *versus* the accumulated milligrams of hydrolyzed protein (HP) that permeated into the recipient cells [30]. From the linear regression analysis, the following were calculated: the steady-state flow rate (*dC / dt*) as mg accumulated in the receiving cell as a function of time (mg/h), using the slope of the curve; with the intercept in the independent coordinate, the Lag time of the steady state region (tL) was estimated, and the apparent permeability coefficient (*Papp*) was obtained by Eq. 5 [31, 32].

$$P_{app} = \left(\frac{dC}{dt} \times \frac{V_{rec}}{AC_0} \right) \quad (5)$$

where, V_{rec} is the volume contained in the recipient cell (mL), A is the effective surface area of the membrane (cm^2), and C_0 is the initial concentration of the hydrolyzed protein in the donor cell (mg/mL).

Confirmation by TEM of Obtaining the Nanoemulsion

To comprehensively analyze the morphology of the droplets obtained and the interface formed in the nanoemulsions, the following systematic procedure was implemented: a suspension of the nanoemulsion loaded with hydrolyzed rice proteins was prepared in distilled water in a 1:1 ratio to ensure adequate dispersion of the particles and facilitate their observation under a microscope. From the prepared suspension, 10 µL were taken and carefully deposited on a nickel grid previously coated with a formvar-based membrane, ensuring the sample was evenly distributed over the surface. The drop deposited on the grid was left to dry at room temperature

for 24 h. Subsequently, the samples were stained using uranyl and lead solutions [33]. Drops of these solutions were applied to the dry sample and left to act for approximately 10 min to improve the micrographs' contrast by increasing the particles' electron density. The treated grid was observed using a transmission electron microscope (JEOL Model JEM 1200 EX, Japan). The micrographs obtained in analog format were developed and digitized using an Epson scanner, obtaining the material in digital format.

Analysis of Interactions Between Formulation Components Using Fourier-transform Infrared Spectroscopy (FT-IR)

NE37, HP, and NE37-HP were studied by FT-IR analysis, following the methodologies established in the scientific literature [34–36]. Data acquisition was performed on IRSpirit FT-IR spectrophotometer, series A22406000512, Shimadzu Corporation, Japan, performing a scan from 600 cm^{-1} to 4000 cm^{-1}.

Results and Discussion

Protein Material

A hydrolyzed protein material was obtained, where the electrophoretic profile showed a predominant band with a molecular weight of 75 kDa.

Determination of the Proportions of the Components

In preliminary tests conducted with 10 test tubes, the fat-soluble phase was colored with Sudan III and the aqueous phase with Methylene Blue (Supplementary Figure S1). These tests focused on formatting Winsor type III emulsions and are characterized by three distinct visible phases: an aqueous phase, an oil phase, and an intermediate phase where the surfactant is distributed. Winsor type III emulsions are crucial in this study because they indicate areas of lower interfacial tension, where the surfactant effectively bridges the oil and water phases. This behavior suggests potential regions for the formation of more stable microemulsions or Winsor type IV emulsions.

The oil ratio of 30:70 was optimal, with a 4% surfactant mixture (SM) yielding the best results. The necessary amount of SM (50:50) was also evaluated, revealing that at high concentrations, the preparations became cloudy, while within the range of 1–8%, a slight halo formed in the middle of the tubes. This halo indicates a uniform distribution of the SM between the two phases, further supporting the formation of Winsor type III emulsions. The visual evidence of this process is depicted in Supplementary Figure S1, which serves as a starting point for subsequent ternary diagram analysis.

HLD Calculation

When calculating the HLD values for the system (Supplementary Table S1), it was evident that salinity influenced the formation of NEs, since stable NEs were observed in regions of lower salinity. With these results, the salinity conditions of the preparation were established on a ternary contour diagram (Fig. 1), which allows viewing the values closest to zero of the HLD obtained for each SM system.

Subsequently, to establish the relationship necessary for obtaining an emulsion with nanometric-sized droplets and a low interfacial tension value to ensure long-term stability, tests were conducted by adjusting the proportion of surfactants and oil. This adjustment aimed to achieve the

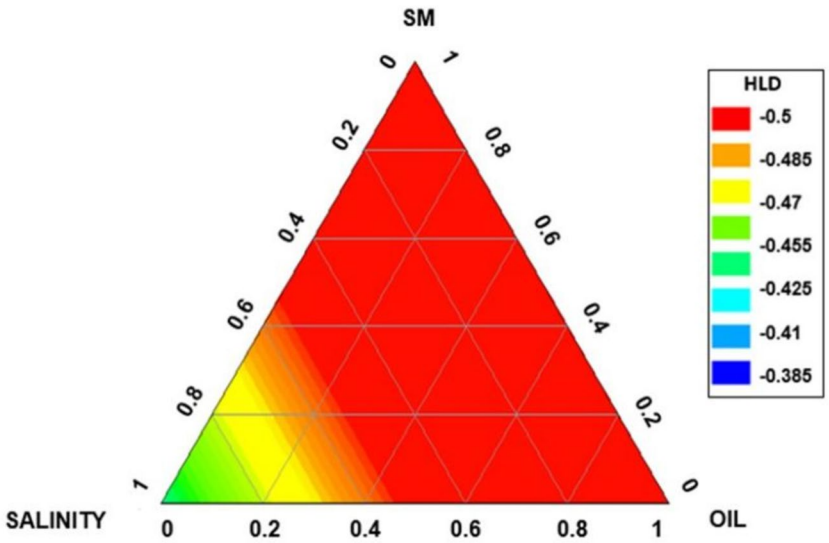

Fig. 1 Contour graphs where the effects of the oil phase ratio, surfactants, and the salinity of the aqueous phase, defined by the HLD values, were evaluated

desired HLD and Cc values. The details of the conducted tests are summarized in Table I.

From the data collected in Table I, a composition diagram was constructed (Fig. 2). This diagram illustrates contour regions that are based on the HLD results, highlighting the formulations that exhibit the desired properties for stability and performance.

Table I Calculated values of Cc and HLD for the NEs

Test	% Oil	Tween 80®	Span 80®	% SM Used for HLD calculation	Cc Mix	HLD
1	80	50	50	10	1.429	1.889
2	80	80	20	10	−0.747	−0.287
3	80	20	80	10	2.588	3.049
4	80	35	65	10	2.085	2.545
5	80	90	10	10	−1.97	−1.51
6	80	100	0	10	−3.7	−3.24
7	80	0	100	10	3.1	3.56
8	80	10	90	10	2.863	3.323
9	80	75	25	10	−0.261	0.199
10	80	71.5	38.54	11	0.537	0.997
11	100	71.5	38.54	7.4	0.537	0.997
12	57	54.6	23.4	7.8	0.164	0.624
13	50	24.5	60.7	8.5	2.302	2.762
14	80	77.25	22.75	10	−0.48	−0.02
15	100	0	0	10	NF	NF
16	80	0	20	10	3.1	3.56
17	80	20	0	10	−3.7	−3.24
18	60	0	40	10	3.1	3.56
19	60	20	20	10	1.422	1.882
20	60	40	0	10	−3.7	−3.24
21	40	0	60	10	3.1	3.56
22	40	20	40	10	2.144	2.604
23	40	40	20	10	0.409	0.869
24	40	60	0	10	−3.7	−3.24
25	20	0	80	10	3.1	3.56
26	20	20	60	10	2.431	2.891
27	20	40	40	10	1.422	1.882
28	20	60	20	10	−0.27	0.19
29	20	80	0	10	−3.7	−3.24
30	0	0	100	10	NF	NF
31	0	20	80	10	NF	NF
32	0	40	60	10	NF	NF
33	0	60	40	10	NF	NF
34	0	80	20	10	NF	NF
35	0	100	0	10	NF	NF
36	20	71.5	38.54	11	0.537	0.997
37	40	71.5	38.54	11	0.537	0.997
38	60	71.5	38.54	11	0.537	0.997
39	90	71.5	38.54	11	0.537	0.997
40	20	77.25	22.75	10	−0.48	−0.02
41	40	77.25	22.75	10	−0.48	−0.02
42	60	77.25	22.75	10	−0.48	−0.02
43	90	77.25	22.75	10	−0.48	−0.02

NF No formation

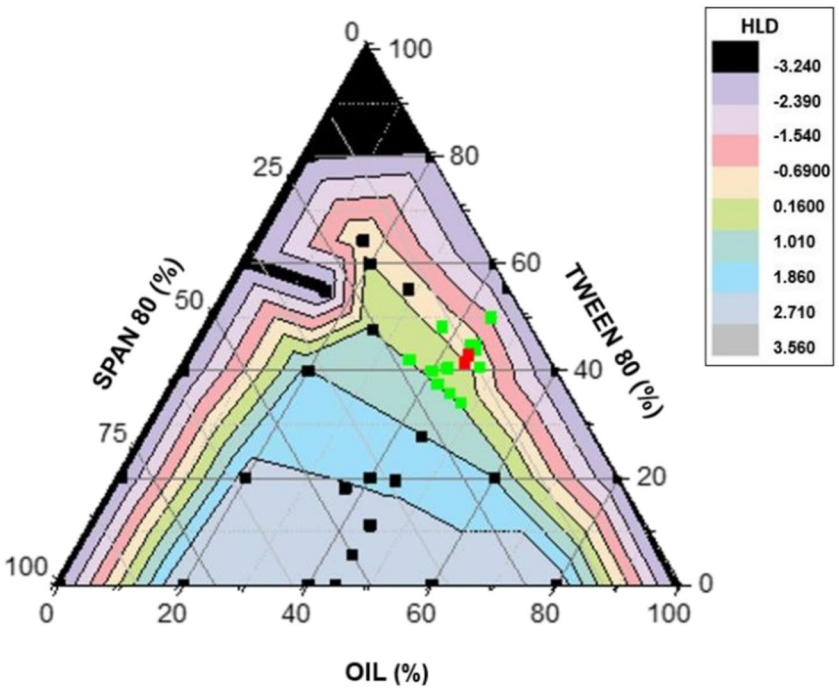

Fig. 2 Pseudo ternary contour diagram, the regions closest to the 0 value for the HLD appear in peach color (HLD between −1.540 and 0.6990), the adjacent areas appear in olive green (HLD between 0.6990 and 0.1600) and pink (HLD between 0.1600 and 1.010). The bright green dots show the tests that met the size and interfacial tension requirements, while in the black dots there was no formation of NEs

In the pseudo ternary composition diagram shown in Fig. 2, it was observed that at the upper and lower limits of each variable (surfactants and oil), the formation of nanoemulsions either did not occur or they were not stable. This observation confirmed the previous results obtained in the optimization process. The location of the majority of the bright green dots in the diagram experimentally demonstrated that an HLD value close to zero represented a low interfacial tension, which in turn allowed for the formation of stable, hyperdispersed nanoemulsion systems.

When the NE formation region was expanded, regions with sizes ranging from 9 to 50 nm (Fig. 3a) and a PDI between 0.24 and 0.33 (Fig. 3b) were observed for all NEs formed in that area.

Based on the results obtained from the ternary composition diagram, six nanoemulsion preparations (PNE1 to PNE6) were selected for further evaluation. These preparations did not exhibit any destabilization after 72 h, as evidenced by the relationship between PS and PDI for PNE 1, 2, 4, 5, 6, and 7 nanoemulsions (Supplementary Figure S2). It was observed that the nanoemulsion labeled as PNE4, containing 77.25% Tween 80 and 22.75% Span 80, exhibited the best characteristics. This preparation was unique in presenting an HLD ≈ 0, which is characteristic of O/W or Windsor III-type nanoemulsions [37]. Additionally, PNE4 exhibited

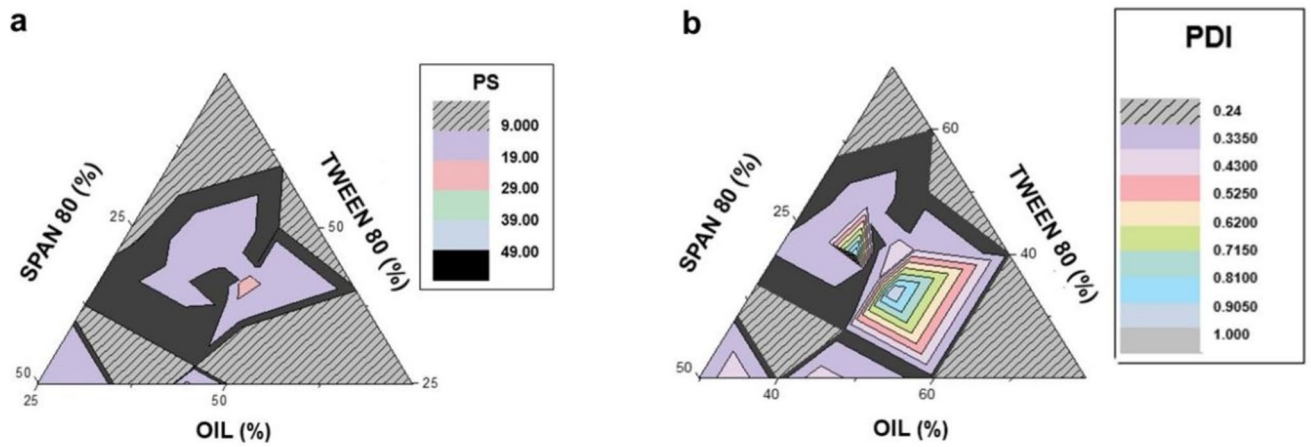

Fig. 3 **a** Variation of particle size in the NE formation zone; **b** PDI variation in the NE formation zone

the smallest droplet size (17.52 ± 0.32 nm). Although all six nanoemulsions presented small droplet sizes, their HLD values differed. This can be attributed to the fact that each surfactant combination provided a different Cc value, resulting in varying HLD values. Furthermore, in the other assays, the nanoemulsions presented an HLD > 0, indicating that they were water-in-oil (W/O) or Windsor I-type nanoemulsions.

Stability Prediction with TSI

Preliminary stability was evaluated for all six PNE preparations through thermal stress testing and detection of variations in the percentage of backscattering (%BS) of the samples over time. Figure 4 showed that in the upper part of the vials for all six tests, there was an increase in %BS, indicating greater backscattering of light compared to the lower and middle areas of the vials. This observation suggested a phenomenon of instability due to the migration of particles to the top, caused by coalescence or aggregation (flocculation), which can lead to long-term creaming.

Interestingly, PNE4 presented the smallest increase in BS in the upper part, suggesting a lower instability level than the other nanoemulsions. These results support the superior stability characteristics of PNE4, which was previously identified as the preparation with the best overall properties based on its HLD value and small droplet size.

These results showed the following scale of instability of the preparations: NE1 > PNE6 > PNE5 > PNE2 > PNE3 > PNE4 (Supplementary Table S2). Instability due to particle migration could be attributed to the high size variability presented by the samples and demonstrated by their high PDI [38, 39]. In this test, again the PNE4 assay showed the lowest TSI values (−0.02) and therefore the highest stability. However, the difference in synergistic stabilization can be attributed to the smaller droplet size and greater uniformity in the size distribution, which may contribute to the better stability of PNE4 by reducing the coalescence process due to the lower collision efficiency [40–42].

The PNE4 preparation was selected as the system to make a better adjustment of the PDI of the formulation with 40 subsequent tests with droplets not loaded with the protein derivative (empty nanoemulsions, ENE), consisting of modifying the oil-SM-water ratio, as presented in Table II, in which the PS and PDI were evaluated.

Table II presents the PS and PDI obtained from the new tests. In these tests, the stability of most of the preparations was insufficient, as visible phase separation was observed in less than 48 h. Consequently, these preparations were excluded from consideration within the stable NE criteria. However, tests ENE31, ENE35, and ENE37 demonstrated favorable results, exhibiting particle sizes below 50 nm and a maximum PDI of 0.31. These results indicated a significant improvement over previous preparations, suggesting that the formulations possess improved stability and characteristics suitable for further development as nanoemulsions.

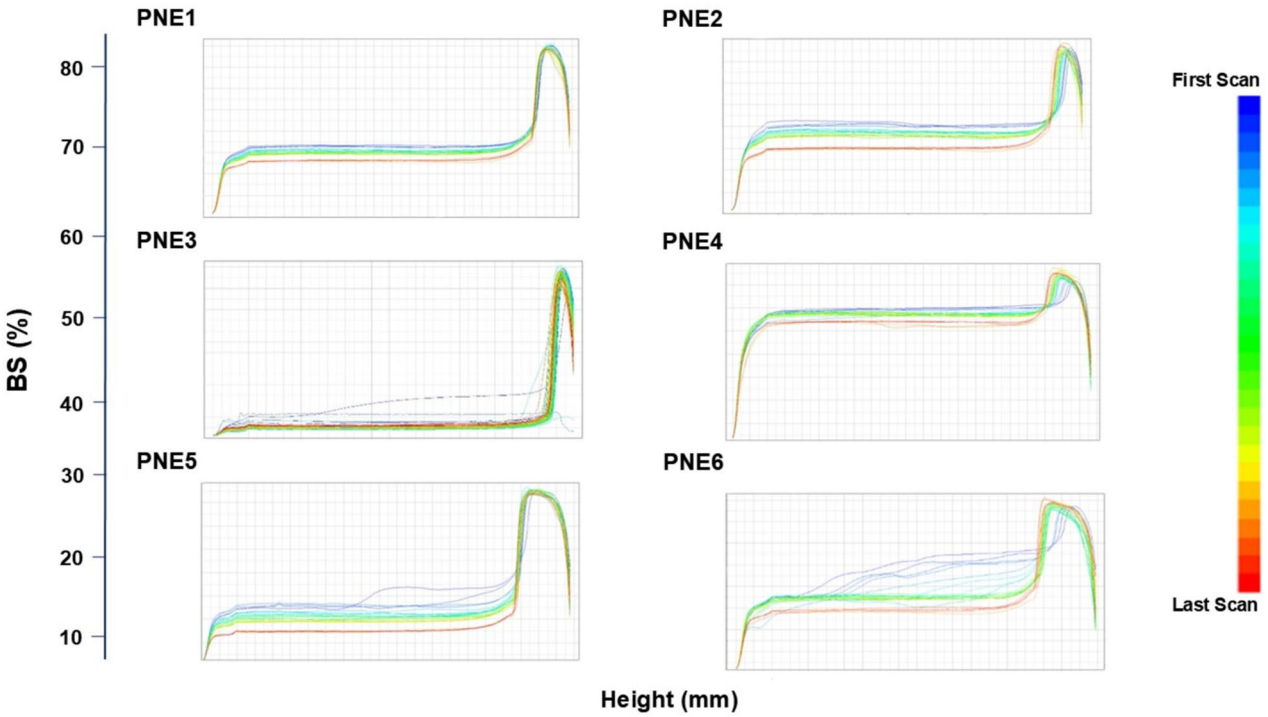

Fig. 4 Variations in backscatter in the PNE1-PNE 6 trials

Table II Summary of the 40 tests of empty nanoemulsions (ENE) in which PS and PDI values were found. (Only the tests where NE formation was observed appear in this Table)

#NE	% Use for diagram			PS (nm)	PDI
	Water	Oil	sunflower		
ENE4	100	0	0	47.62	0.21
ENE6	80	0	20	696.87	0.88
ENE7	80	20	0	42.55	0.19
ENE8	60	0	40	7505	0.65
ENE10	60	40	0	48.29	0.36
ENE12	40	20	40	52.21	0.49
ENE13	40	40	20	136.1	0.68
ENE30	45	45	10	30.2	0.205
ENE31	**45**	**40**	**15**	**43.62**	**0.35**
ENE32	59	29	10	225	0.021
ENE35	**50**	**30**	**20**	**45.7**	**0.21**
ENE37	**50**	**40**	**10**	**47.25**	**0.21**
ENE38	70	30	0	600.3	0.225
ENE39	60	10	30	29.15	0.29

PS particle size, *PDI* polydispersity index

Based on these results, contour diagrams for PS and PDI were constructed. Figure 5a and b illustrate a similar asymmetric performance. It can be observed that within the range of 0 to 30% water and above 60% oil, the formation of emulsions on a nanometric scale does not occur, and the PDI values are significantly high [43]. This phenomenon can be explained by the vertices of the ternary diagram, where there are excessively high quantities of one component and a complete absence of another. However, it is anticipated that this performance will improve as the values of the variables are centered, leading to more balanced compositions that facilitate the formation of stable nanoemulsions with optimal PS and PDI characteristics [44].

In Fig. 5a, where the pink regions of the ternary diagram (PS ranging between 10 to 133 nm) are superimposed with the navy-blue region of Fig. 5b (PDI between 0.14 and 0.26), three preparations were demarcated that remained stable after 48 h of preparation (ENE31, ENE35 and ENE37), and that delimit a region of formation of stable emulsions, which satisfies the criteria required for NE [45].

Figure 6 illustrates the variations in backscattering for the ENE31, ENE35, and ENE37 emulsions. A slight decrease in the percentage of backscattering (%BS) was observed in the lower area of the vials for the ENE31 and ENE37 tests, which may indicate a potential clearing in this region over the long term, consistent with the migration of particles towards the middle and upper zones of the vials. In contrast, the ENE35 preparation exhibited high variability in the backscatter measurements across all areas. Coupled with the TSI data presented in Supplementary Table S3, these observations conclude that ENE35 is a highly unstable nanoemulsion. This instability suggests that further formulation optimization may be necessary to enhance its stability and performance [46, 47].

The ENE37 nanoemulsion was the test that presented the lowest TSI value after 72 h (Supplementary Table S3), and did not show, macroscopically, any associated instability phenomenon in the D-65 light booth test, therefore, this preparation was taken as a supporting frame or base formula for the incorporation of protein derivatives.

Evaluation of the Effects of the Addition of Protein Derivatives to the ENEs

The consolidated tests conducted on the ENE37 emulsions, including before and after loading with 1%

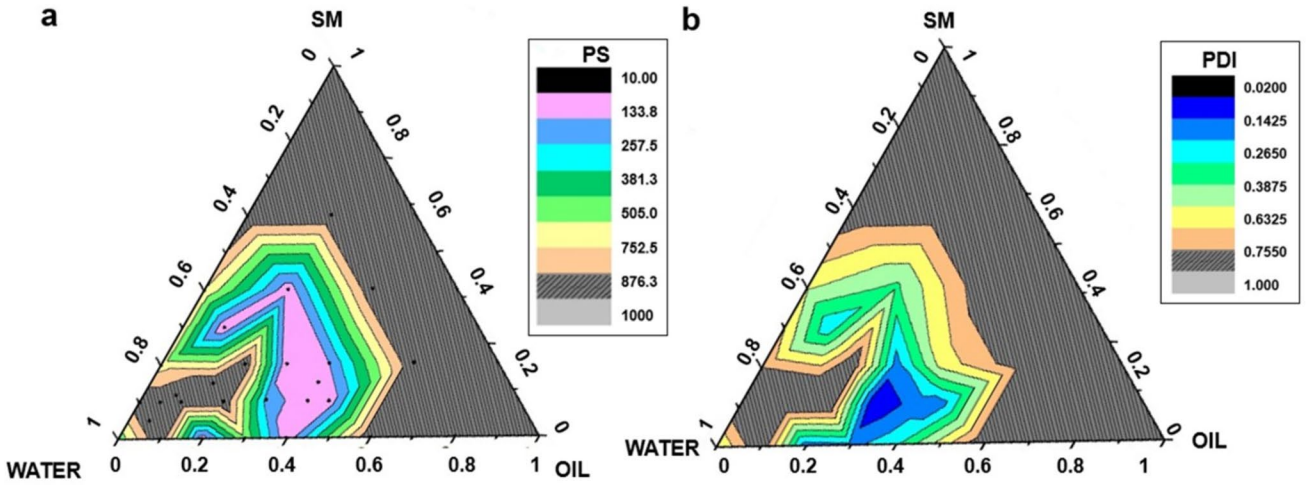

Fig. 5 Variation in the emulsion formation zone of ENEs: **a** PS and **b** PDI

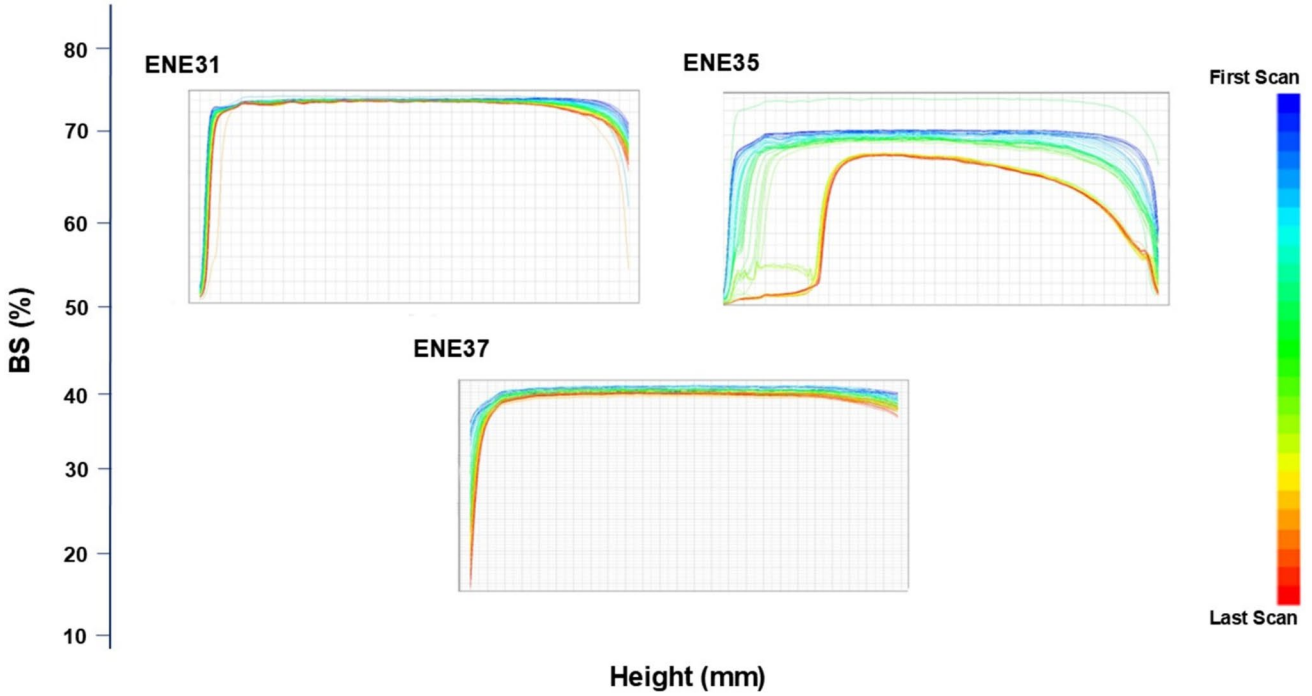

Fig. 6 Variations in the backscattering of nanoemulsions ENE31, ENE35 and ENE37

hydrolyzed straw protein (NE37-HP) are detailed in Supplementary Table S4. The results indicated minimal variation in the PS and PDI values. Notably, an increase in the zeta potential was observed, indicating a negative charge. This can be attributed to the zwitterionic behavior of the amino acids present in the hydrolyzed protein [47], which may enhance emulsion stability by generating greater electrostatic repulsion between the globules [48, 49].

When evaluating the addition of dyes, the NE37-HP preparation maintained its classification as an O/W nanoemulsion, as confirmed by the fluorescence pattern observed in the microphotographed samples [21].

The dispersibility and dilution tests for the ENE37 nanoemulsion revealed that at a dilution of 1 in 16, there was noticeable migration towards the surface of the test tube. In contrast, the NE37-HP formulation did not exhibit this behavior, even at dilutions of 1 in 28. This suggests that NE37-HP is more stable upon the addition of water and can withstand significantly higher dilutions without undergoing phase inversion phenomena [22].

The improved stability of the NE37-HP emulsions during dilution can be attributed to the enhanced electrostatic stability conferred by the protein derivatives, which is directly influenced by the charges of the amino acid residues present in the formulation.

Rheological Characterization of the NE37-HP Formulation

Rheological Properties

Figure 7 illustrates a diagram of the relationship between stress rate and shear. The shear thinning behavior of the NE was observed. Specifically, the viscosity decreased at a shear rate of 0.01 s^{-1}, indicating pseudoplastic behavior. This phenomenon can be attributed to the loss of closed packing and the breaking of intermolecular bonds, suggesting a stabilizing effect exerted by the protein derivatives [50].

Within the shear rate range of 0.1 to 10 s^{-1}, the NE experienced a significant drop in viscosity, indicating that bond breaking was occurring. Following this initial decrease, the viscosity remained relatively constant up to a shear rate of 100 s^{-1} [24]. This behavior highlights the non-Newtonian characteristics of the formulation, which are influenced by the interactions among the components and the stabilizing effects of the protein derivatives.

Pseudoplastic fluid was analyzed, applying the Newton, Power Law, Herschel- Bulkley, Bingham, and Casson models to the flow curve of the NE37-PH, as described in Supplementary Table S5 [51, 52].

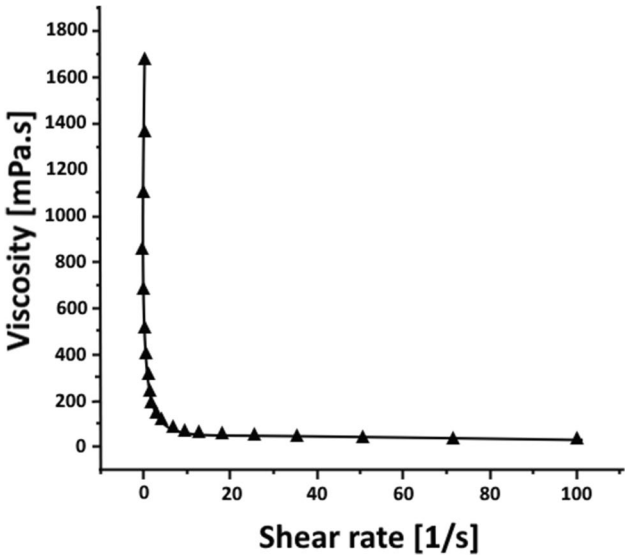

Fig. 7 Flow curves for NE37-HP

All models confirmed that NE37-HP experienced shear thinning since in all of them, the flow behavior index (N) was less than or equal to 1 (Table II). Starting from the highest correlation coefficient (r^2), the best-fitted model was the Casson model, which was used to evaluate the rheological behavior. The apparent viscosity (η), at a shear rate at 60 s^{-1} calculated with Eq. 2, was 8.792 (Pa.s) for NE37-HP. With the creep threshold parameter (σ 0) Modified Casson defined the minimum shear stress required to start the flow, and in this case, suggested that the NE requires a minimum stress to start the flow [53]. These rheological results were complemented with amplitude and frequency oscillatory tests [23].

Oscillatory Amplitude Sweeps

Figure 8a shows the results that represent the variation of the storage (G′) and loss moduli (G″) with the shear stress (γ). Amplitude sweep tests were performed in the strain range covering small and large amplitude strain regimes to understand the viscoelastic behavior. However, a linear viscoelastic region (RLVE) was not observed for the NE. The two modules differed only in low shear stress, where, above the crossover stress, G″ exceeded G′ after being lower, which indicated that the transition is predominantly pseudoplastic behavior. Subsequently, the constant and parallel values of G′ and G″ were a consequence of the lack of a defined internal structure of the sample.

Additionally, comparative tests were carried out for monitoring the viscoelastic response from the modules G' and G'', while applying a swept frequency to detect deformations [54, 55]. Figure 8b showed values for the two functions, using a voltage of 0.1%, where it was observed that at frequencies lower than 20 rad/s, both modules presented an increasing trend, but with a lower loss module value, indicating an initial elastic behavior, then radically inverting (G´´ > > G´) as the frequency increases, revealing a more viscous than elastic behavior. These results were similar to those reported in O/W emulsions stabilized with soy protein and could be attributed to the presence of the hydrolyzed protein, possibly due to the gel formation capacity exhibited by the proteins, and that to stabilize to the emulsions [56, 57].

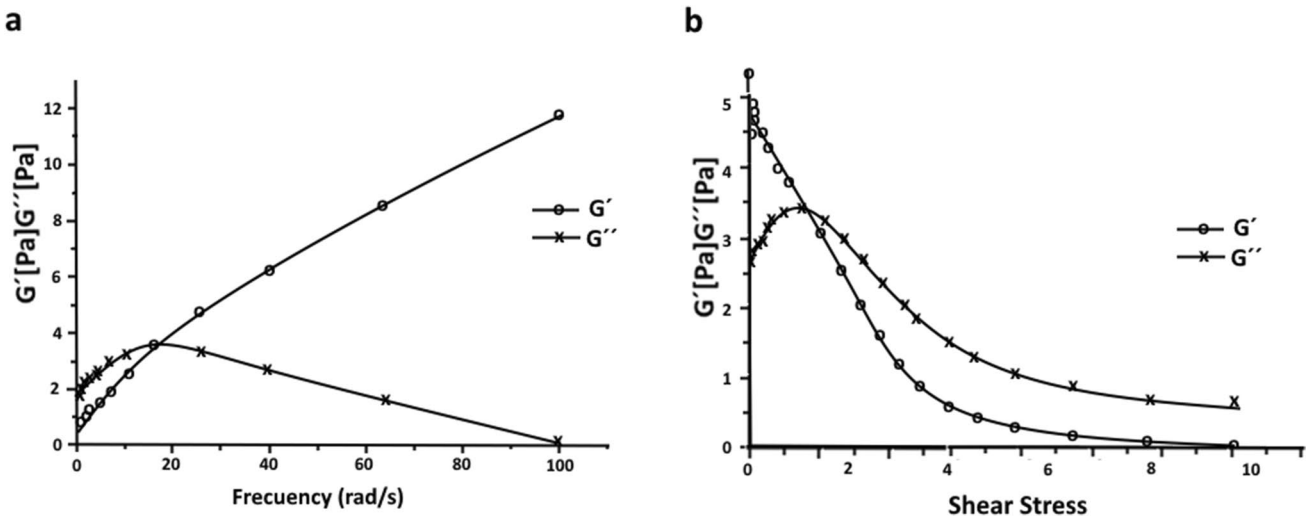

Fig. 8 **a** Shear stress amplitude sweeps *vs* G' and G''; **b** Frequency sweeps rad/s *vs* G' and G'' for the ENE37-HP nanoemulsion

Stability of Protein NEs

Estimation of Preliminary Stability by the TSI Method

The BS measurements for the NE37-HP nanoemulsion indicated a decrease in BS values over time, which may suggest a clarification process occurring in the lower area of the measuring cell [58, 59]. However, no macroscopic changes in appearance, color, or odor were observed in either nanoemulsion after subjecting them to six cycles of temperature fluctuations between 5 °C and 40 °C, each lasting 48 h. Following this, a centrifugation test was conducted at 3000 rpm for 30 min, and the emulsions were subsequently tested under alternating ambient and refrigeration conditions.

Based on these assessments, it can be concluded that the NE37-HP emulsions exhibited stability. Although phenomena such as particle migration may have occurred, these changes were not readily apparent to the human eye. This suggests that the emulsions maintained their structural integrity and performance despite the stress conditions applied during the stability tests [60, 61].

To monitor the stability of the NE37-HP formulation, an analysis was conducted using the PS and PDI values from Table III as variables. Various kinetic models were evaluated to determine which mathematical approach best explains the stability behavior of the formulation over time. This analysis was performed using Statgraphics Centurion 19® software (v. 19.1.2), allowing us to understand how these parameters relate to the stability of NE.

It was found that the kinetic trend of PS and PDI *vs* time fit a *double inverse model*, where PS = 1 / (0.0173 + 0.0029/ week), with an R^2 of 99.5% and for the PDI = 1/ (3.335 + 0.797/ week), with an R^2 of 88.7%. With these models, it could be inferred that for 104 weeks (being 2 years the minimum shelf life commonly accepted for these products), the preparation could be preserved with a PS of 57.7 nm and with a PDI of 0.299.

Table III Monitoring the stability index based on the increase in PS and PDI, after 5 weeks of testing for the NE37-HP preparation

Time	PS (nm)	PDI
Initial	49.51 ± 0.307	0.245 ± 0.002
Week 2	53.51 ± 0.645	0.280 ± 0.026
Week 3	54.43 ± 0.071	0.275 ± 0.002
Week 4	55.56 ± 0.245	0.289 ± 0.005
Week 5	56.08 ± 0.578	0.282 ± 0.005

PS particle size, *PDI* polydispersity index

In vitro Evaluation of the Apparent Permeability of NEs

The test for determining the prediction of dermal permeation was performed in Franz diffusion cells of the hydrolyzed protein loaded in the NE, using Strat-M® as a membrane. The quantities obtained in the recipient cells were measured, using the reagent of Bradford and the profile of the amount of HP accumulated in the recipient cell as a function of time. The calculation of the accumulated permeability (p_{acum}) appears in Table IV, taking samples of 0.2 mL, and with a volume in the receiving cell of 11.5 mL.

From the data in Table IV, a linear regression curve was constructed (Supplementary Figure S3) and the steady flow data (dC/dt) of 0.011 mg/mL/h (slope of the curve) were obtained, and the Lag time of the steady state region (tL) of 0.774 h. The maximum apparent accumulated permeation was calculated by applying Eq. 5, taking a volume in the receiving compartment (Vrec) of 10.5 mL, 0.2 mL volume in each sampling (Vj), and with a membrane area (Amemb) of 3.89 cm^2. In this case, due to the quantification limits of the analyte method used, and since the results are assumed as a zero-order process, where the permeation rate is independent of the concentration of the protein material, the initial concentration (C0) was increased of 8.8 mg/mL of the hydrolyzed protein to facilitate the detection capacity of the analyte in the donor cell; with these data, it was determined that the Papp was 20.14 µg/cm^2.h (SD ± 0.01), indicating the intrinsic ease of the HP contained in NE37-HP to diffuse through the membrane Strat M and those test conditions.

Table IV Cumulative permeability for the NE37-HP test

Time (min)	mg/mL	Accumulated Permeability(mg)
0	0	0
30	0.004086	0.047809
60	0.026175	0.306248
90	0.047962	0.561152
120	0.064824	0.758444
150	0.094842	1.109648
180	0.110878	1.297273
210	0.143348	1.677177
240	0.15695	1.836319
270	0.193693	2.266208
300	0.227727	2.664403
330	0.286173	3.34822
360	0.328757	3.846459

Analysis by TEM

The TEM micrographs (Supplementary Figure S4) showed that the nanoemulsion contains homogeneously dispersed spheroidal droplets surrounded by portions of the non-encapsulated protein derivatives, indicating its stability. In the enlarged inner inset of Supplementary Figure S4(a), representative droplets of the NE37-HP formation are shown, with a dark appearance, due to the staining of the protein derivatives with uracil and lead, with a compact appearance and a rough surface. The difference in contrast also allows us to observe a well-defined interface in the envelope around the droplets, as seen in the inset of Supplementary Figure S4(b), which may indicate a stable emulsion, composed of the surfactants and protein derivatives (darker part).

Analysis by FT-IR

The peak values of FT-IR spectra for HP (A), NE37 (B), and NE37-HP (C) are illustrated in Supplementary Figure S5. The FT-IR spectrum of the rice protein hydrolysates (spectrum A) reveals a relatively simple profile, indicating the presence of key functional groups. Notably, the broad peak at 3310 cm^{-1} corresponds to O–H stretching vibrations, suggesting a significant presence of hydroxyl groups. This indicates the hydrophilic nature of the hydrolysates, which may enhance their solubility and interaction with water in the nanoemulsion matrix. The peak at 1634 cm^{-1} is attributed to H–O-H stretching vibrations and overlapping C-N bands associated with amines, further confirming the presence of amino acids and peptides resulting from hydrolysis [34].

In spectra B (NE37) and C (NE37-HP), additional peaks provide insights into the interactions and complexity of the nanoemulsion. Peaks at 2920 cm^{-1} and 2850 cm^{-1} correspond to asymmetric and symmetric C-H bond stretching vibrations, respectively. These peaks are characteristic of aliphatic hydrocarbons found in sunflower oil and surfactants, suggesting effective emulsification processes that contribute to the stability of the nanoemulsion. The peak at 1740 cm^{-1}, attributed to C-O stretching of carbonyls, indicates the presence of ester groups commonly found in surfactants like polysorbate 80 and Twin 80. The intensity of this peak reflects the complexity of components within the nanoformulation, suggesting that interactions between oil droplets and surfactants may stabilize the emulsion by reducing interfacial tension [35, 36].

The peaks at 1460 cm^{-1} and 1350 cm^{-1} correspond to angular deformation vibrations of C-H bonds and C-H bending vibrations, respectively. These vibrations correspond to methyl and methylene groups prevalent in both surfactants and oils. Their presence suggests that these components are well integrated into the nanoemulsion structure, potentially enhancing stability through steric hindrance [35, 36].

Additionally, peaks at 1150 cm^{-1} and 1100 cm^{-1} are attributed to C-O bending vibrations. These peaks highlight interactions between various functional groups within the formulation, particularly between hydrophilic surfactants and hydrophobic oil phases. Such interactions are pivotal for maintaining emulsion stability by preventing the coalescence of oil droplets [36].

In summary, the nanoemulsion ENE37 (formulation consisting of 50% water, 40% sunflower oil, and 10% surfactant mixtures), exhibited the highest stability in terms of particle size, measuring 47.25 nm, with a PDI of 0.21. Our results are comparable with values previously reported in the literature, including for nanoemulsions produced by high-energy methods, such as high-pressure homogenizers [62, 63].

Backscattering tests revealed a slight decrease in light scattering at the bottom of the vials, indicating mild clarification without phase separation. Its low TSI confirmed high stability, with minimal tendency for coalescence or flocculation. Furthermore, ENE37 demonstrated excellent dispersion and resistance to separation in dilution tests (up to 1:28), maintaining its structural integrity without any evidence of phase inversion, suggesting stability and support for infinite dilutions [22].

Upon incorporating hydrolyzed rice straw protein into ENE37 to create the formulation NE37-HP, an additional improvement in stability was observed. The hydrolyzed protein increased the zeta potential to negative values, attributed to the zwitterionic behavior of the amino acids, which generates greater electrostatic repulsion between droplets and prevents aggregation. The results are consistent with findings from other researchers, highlighting the stabilizing properties of protein emulsions and their plant-derived hydrolysates. This is attributed to their ability to generate both steric and electrostatic repulsive interactions, which enhance emulsion stability [64].

NE37-HP exhibited excellent stability in dilutions, maintaining its structure even at diluted concentrations without phase inversion. Fluorescence studies confirmed that NE37-HP remained an O/W nanoemulsion, with good protein distribution in the aqueous phase, coinciding with the established pattern for an O/W type emulsion [21].

From a rheological perspective, NE37-HP displayed shear-thinning behavior, which is advantageous for topical applications, and showed increased perceived consistency—an important attribute for user sensory experience [23].

In permeability tests using Strat-M® membranes with Franz cells, NE37-HP demonstrated good diffusion capacity of the hydrolyzed protein, achieving an accumulated permeability of 20.14 $\mu g/cm^2.h$. This result confirms that the permeability of active ingredients through the skin can be enhanced using nanometric formulations. The small particle size of these formulations facilitates the penetration of active ingredients through the stratum corneum, regardless

of whether they are hydrophilic or possess a high molecular weight [29, 65]. This supports its potential as an efficient carrier for bioactive compounds in skin applications.

Conclusions

In this research, the HLD method was pivotal in developing a stable O/W nanoemulsion for dermal delivery of protein hydrolysates. The strategic selection of Polysorbate 80 and sorbitan oleate 80 optimized the emulsification process, achieving stability with minimal energy input through a single high-shear homogenization cycle. Although this nanoemulsion included protein hydrolysate, the formulation maintained consistent viscoelastic properties, enhancing sensory perception and suggesting increased efficacy.

The obtained nanoemulsions demonstrated exceptional stability over a two-year shelf life, with minor creaming observed, indicating its potential for long-term application. Using sunflower oil and rice straw-derived protein hydrolysates supports antioxidant benefits and enhances dermal absorption. The results highlight the importance of innovative, sustainable formulation strategies in delivering bioactive compounds effectively in cosmetic contexts.

Abbreviations Amemb: Membrane area; BS: Backscatter; Cc: Characteristic curvature of the surfactants; C0: Initial concentration; Cys: Cysteine; EACN: Equivalent Alkane Carbon Number; EDTA: Ethylenediamine tetraacetic acid; *dC / dt*: Steady-state flow rate; DLS: Dynamic Light Scattering; DPPH: 2,2-Diphenyl-1-picrylhydrazyl; ENE: Empty nanoemulsions; FT-IR: Fourier-transform infrared spectroscopy; G′: Variation of the storage; G″: Loss moduli; H: Height; His: Histidine; HLB: Hydrophile-Lipophile Balance; HLD: Hydrophilic-Lipophilic Deviation; HP: Hydrolyzed protein; K: Consistency coefficient or proportionality constant; LVR: Linear viscoelastic region; Lys: Lysine; n: Flow behavior index; η: Viscosity; N: Flow behavior index; NE: Nanoemulsion; NEs: Nanoemulsions; NF: No formation; Met: Methionine; MW: Molecular weight; O/W: Oil-in-water; *Papp*: Apparent permeability coefficient; PDI: Polydispersity index; PNE: Nanoemulsion preparation; Pro: Proline; PS: Particle size; RLVE: Linear viscoelastic region; t: Time; tL: Lag time; T or T°: Temperature; TEM: Transmission electron microscopy; Trp: Tryptophan; TSI: Turbiscan stability index; Vj: Volume in each sampling; Vrec: Volume in the receiving compartment; γ: Shear stress; $\dot{\gamma}$: Strain rate; Tyr: Tyrosine; S: Salinity; SM: Surfactant mixture; W/O: Water-in-oil

Supplementary Information The online version contains supplementary material available at https://doi.org/10.1208/s12249-025-03043-5.

Acknowledgements The authors acknowledge the Committee for the Development of Research (CODI) at the University of Antioquia for their financial support through the 2017 programmatic announcement and the Electron Microscopy Unit/University of Cauca-Colombia for acquiring TEM images.

Author Contributions PV-E: Writing – original draft, Investigation, Data collection, Conceptualization. PQ-R: Writing – review & editing, Data collection. OF-A: Writing – review & editing, Project administration, Funding acquisition, Formal analysis, Data curation, Conceptualization.

Funding Open Access funding provided by Colombia Consortium.

Data Availability This published article and supplementary material include all data generated or analyzed during the research. The data of this study are available from the corresponding author upon reasonable request.

Declarations

Ethics Approval and Consent to Participate This article does not contain any studies involving animals performed by any of the authors. This article does not contain any studies involving human participants performed by any of the authors.

Consent for Publication Not applicable.

Competing Interests The authors report no conflicts of interest. The authors alone are responsible for the content and writing of this article.

References

1. Morganti P, Gao X, Vukovic N, Gagliardini A, Lohani A, Morganti G. Food loss and food waste for green cosmetics and medical devices for a cleaner planet. Cosmetics. 2022;9(1):19. https://doi.org/10.3390/cosmetics9010019
2. Mishra B, Mohanta YK, Reddy CN, Reddy SDM, Mandal SK, Yadavalli R, Sarma H. Valorization of agro-industrial biowaste to biomaterials: an innovative circular bioeconomy approach. Circ Econ. 2023;2(3):100050.
3. Peanparkdee M, Iwamoto S. Bioactive compounds from by-products of rice cultivation and rice processing: extraction and application in the food and pharmaceutical industries. Trends Food Sci Technol. 2019;86:109–17.
4. de Miranda MS, Fonseca ML, Lima A, de Moraes TF, Rodrigues FA. Environmental impacts of rice cultivation. Am J Plant Sci. 2015;6(12):2009.
5. Pang B, Zhou T, Cao XF, Zhao BC, Sun Z, Liu X, Chen YY, Yuan TQ. Performance and environmental implication assessments of green bio-composite from rice straw and bamboo. J Clean Prod. 2022;375:134037.
6. Vargas-Escobar P, Flórez-Acosta O, Corrales-García LL. Renewing the potential of rice crop residues as value-added products in the cosmetics industry. Heliyon. 2024;10(7):e28402.
7. Saito K, Jin DH, Ogawa T, Muramoto K, Hatakeyama E, Yasuhara T, Nokihara K. Antioxidative properties of tripeptide libraries prepared by the combinatorial chemistry. J Agric Food Chem. 2003;51(12):3668.

8. Samaranayaka AG, Li-Chan EC. Food-derived peptidic antioxidants: a review of their production, assessment, and potential applications. J Funct Foods. 2011;3(4):229–54.
9. Singh TP, Siddiqi RA, Sogi DS. Enzymatic modification of rice bran protein: Impact on structural, antioxidant and functional properties. Lwt. 2021;138:110648.
10. Klost M, Drusch S. Functionalisation of pea protein by tryptic hydrolysis–Characterisation of interfacial and functional properties. Food Hydrocoll. 2019;86:134–40.
11. O'Regan J, Mulvihill DM. Sodium caseinate–maltodextrin conjugate hydrolysates: preparation, characterisation and some functional properties. Food Chem. 2010;123(1):21–31.
12. Gomes MHG, Kurozawa LE. Performance of rice protein hydrolysates as a stabilizing agent on oil-in-water emulsions. Food Res Int. 2023;172:113099.
13. Faria-Silva AC, Mota AL, Costa AM, Silva AM, Ascenso A, Reis C, Simões S. Application of natural raw materials for development of cosmetics through nanotechnology. In Nanotechnology for the Preparation of Cosmetics Using Plant-Based Extracts. Elsevier; 2022. pp. 157–201.
14. Gaikwad R, Shinde A. Overview of nanoemulsion preparation methods, characterization techniques and applications. Asian J Pharm Technol. 2022;12(4):329.
15. Pateiro M, Gómez B, Munekata PES, Barba FJ, Putnik P, Kovačević DB, Lorenzo JM. Nanoencapsulation of promising bioactive compounds to improve their absorption, stability, functionality and the appearance of the final food products. Molecules. 2021;26(6):1547.
16. Chanthathamrongsiri N, Prompanya C, Leelakanok N, Jiangseubchatveera N, Semangoen T, Nuurai P, Khawsuk W, Petchsomrit A. Rice extract: antioxidant activities and formulations. J Appl Pharm Sci. 2022;12(12):126.
17. Quintero-Rincón P, Mesa-Arango AC, Flórez-Acosta OA, Zapata-Zapata C, Stashenko EE, Pino-Benítez N. Exploring the potential of extracts from *Sloanea medusula* and *S. calva*: formulating two skincare gels with antioxidant, sun protective factor, and anti-*Candida albicans* activities. Pharmaceuticals. 2023;16(7):990.
18. Kiran SK, Acosta EJ. HLD–NAC and the formation and stability of emulsions near the phase inversion point. Ind Eng Chem Res. 2015;54(25):6467.
19. Salager JL, Antón R, Bullón J, Forgiarini A, Marquez R. How to use the normalized hydrophilic-lipophilic deviation (HLDN) concept for the formulation of equilibrated and emulsified surfactant-oil-water systems for cosmetics and pharmaceutical products. Cosmetics. 2020;7(3):57.
20. Abbott, S. Surfactant Science: Principles and Practice. DEStech Publications: Lancaster, PA, USA, 2015; ISBN 9781605954844.
21. Harika K, Debnath S. Formulation and evaluation of nanoemulsion of amphotericin B. Int J Novel Trends Pharm Sci. 2015;5(4):114.
22. Gurpreet K, Singh SK. Review of nanoemulsion formulation and characterization techniques. Indian J Pharm Sci. 2018;80(5):781.
23. Fuentes K, Matamala C, Martínez N, Zúñiga RN, Troncoso E. Comparative study of physicochemical properties of nanoemulsions fabricated with natural and synthetic surfactants. Processes. 2021;9(11):2002.
24. Sarkar A, Goh KK, Singh H. Properties of oil-in-water emulsions stabilized by β-lactoglobulin in simulated gastric fluid as influenced by ionic strength and presence of mucin. Food Hydrocoll. 2010;24(5):534.
25. Pillai P, Saw RK, Mandal A. Formulation and characterization of ionic liquid-based nanoemulsion for enhanced oil recovery applications. J Mol Liq. 2024;397:124189.
26. Mao L, Yang J, Xu D, Yuan F, Gao Y. Effects of homogenization models and emulsifiers on the physicochemical properties of β-carotene nanoemulsions. J Dispers Sci Technol. 2010;31(7):986–93.
27. Ullah N, Amin A, Alamoudi RA, Rasheed SA, Alamoudi RA, Nawaz A, Raza M, Nawaz T, Ishtiaq S, Abbas SS. Fabrication and optimization of essential-oil-loaded nanoemulsion using box-behnken design against staphylococos aureus and staphylococos epidermidis isolated from oral cavity. Pharmaceutics. 2022;14(8):1640.
28. Samson S, Basri M, Masoumi HRF, Karjiban RA, Malek EA. Design and development of a nanoemulsion system containing copper peptide by D-optimal mixture design and evaluation of its physicochemical properties. RSC Adv. 2016;6(22):17845–56.
29. Bernardi DS, Pereira TA, Maciel NR, Bortoloto J, Viera GS, Oliveira GC, Rocha-Filho PA. Formation and stability of oil-in-water nanoemulsions containing rice bran oil: in vitro and in vivo assessments. J Nanobiotechnol. 2011;9:1–9.
30. Lent EM, Maistros KJ, Oyler JM. *In vitro* dermal absorption of carfentanil. Toxicol In Vitro. 2020;62:104696.
31. Iizhar SA, Syed IA, Satar R, Ansari SA. *In vitro* assessment of pharmaceutical potential of ethosomes entrapped with terbinafine hydrochloride. J Adv Res. 2016;7(3):453–61.
32. Yang Y, Zhao Y, Yu A, Sun D, Yu LX. Chapter 12 - Oral drug absorption: Evaluation and prediction. In: Qiu Y, Chen Y, Zhang GGZ, Yu L, Mantri RV, editors. Developing solid oral dosage forms. 2nd ed. Academic Press; 2017. pp. 331–354. https://doi.org/10.1016/B978-0-12-802447-8.00012-1.
33. Klang V, Matsko NB, Valenta C, Hofer F. Electron microscopy of nanoemulsions: an essential tool for characterisation and stability assessment. Micron. 2012;43(2–3):85–103.
34. Agnish S, Sharma AD, Kaur I. Nanoemulsions (O/W) containing *Cymbopogon pendulus essential* oil: development, characterization, stability study, and evaluation of *in vitro* antibacterial, anti-inflammatory, anti-diabetic activities. BioNanoScience. 2022;12(2):540–54.
35. Viana RB, da Silva AB, Pimentel AS. Infrared spectroscopy of anionic, cationic, and zwitterionic surfactants. Adv Phys Chem. 2012;2012(1):903272.
36. Sharma AD, Kaur I, Chauhan A (2024) Anti-aspergillosis and anti-mucormycosis potential of eucalyptus essential oil based O/W nanoemulsions containing azole based drugs from Eucalyptus globulus. J Umm Al-Qura Univ Appl Sci. 2024;10:313–29. https://doi.org/10.1007/s43994-023-00108-8
37. Salager JL, Antón RE, Anderez JM, Aubry JM. Formulation des microémulsions par la méthode du HLD. Editions TI. 2001. pp. 1–20. https://www.researchgate.net/profile/Jean-Louis-Salager/publication/284581087_Formulation_des_microemulsions_par_la_methode_HLD/links/57c0bc8508aeb95224d4a696/Formulation-des-micro-emulsions-par-lamethode-HLD.pdf
38. Kim YJ, Kim BK, Lee MH. Effect of small molecular surfactants on physical, turbidimetric, and rheological properties of pickering nanoemulsions stabilized with whey protein isolate. Food Biosci. 2023;51:102214.
39. Villalobos-Espinosa JC, García-Armenta E, Alamilla-Beltrán L, Quintanilla-Carvajal MX, Azuara-Nieto E, Hernández-Sánchez H, Perea-Flores MJ, Gutiérrez-López GF. Effect of pumping and atomisation on the stability of oil/water emulsions. J Food Eng. 2022;327:111056.
40. Chen Z, Zhang S, Li Z, Ma G, Su Z. Construction of a stable w/o nano-emulsion as a potential adjuvant for foot and mouth disease virus vaccine. Artif Cells Nanomed Biotechnol. 2017;45(5):897.
41. Sanchez A, García MC, Martín-Piñero MJ, Muñoz J, Alfaro-Rodríguez MC. Elaboration and characterization of nanoemulsion with orange essential oil and pectin. J Sci Food Agric. 2022;102(9):3543.

42. Peng F, Ke Y, Lu S, Zhao Y, Hu X, Deng Q. Anion amphiphilic random copolymers and their performance as stabilizers for O/W nanoemulsions. RSC Adv. 2019;9(26):14692.
43. Rave MC, Echeverri JD, Salamanca CH. Improvement of the physical stability of oil-in-water nanoemulsions elaborated with Sacha inchi oil employing ultra-high-pressure homogenization. J Food Eng. 2020;273:109801.
44. Chong WT, Tan CP, Cheah YK, Lajis AFB, Habi Mat Dian NL, Kanagaratnam S, Lai OM. Optimization of process parameters in preparation of tocotrienol-rich red palm oil-based nanoemulsion stabilized by Tween80-Span 80 using response surface methodology. PLoS One. 2018;13(8):e0202771.
45. Kumar H, Kumar V. Ultrasonication assisted formation and stability of water-in-oil nanoemulsions: optimization and ternary diagram analysis. Ultrason Sonochem. 2018;49:79–88.
46. Dong T, Norisuye T, Nakanishi H, Tran-Cong-Miyata Q. Particle size distribution analysis of oil-in-water emulsions using static and dynamic ultrasound scattering techniques. Ultrasonics. 2020;108:106117.
47. Choi SJ, Won JW, Park KM, Chang PS. A new method for determining the emulsion stability index by backscattering light detection. J Food Process Eng. 2014;37(3):229–36.
48. Sharifi F, Jahangiri M, Nazir I, Asim MH, Ebrahimnejad P, Hupfauf A, Gust R, Bernkop-Schnürch A. Zeta potential changing nanoemulsions based on a simple zwitterion. J Colloid Interface Sci. 2021;585:126–37.
49. Kamble S, Agrawal S, Cherumukkil S, Sharma V, Jasra RV, Munshi P. Revisiting zeta potential, the key feature of interfacial phenomena, with applications and recent advancements. ChemistrySelect. 2022;7(1):e202103084.
50. Smulders PEA. Formation and stability of emulsions made with proteins and peptides [PhD thesis]. Wageningen, The Netherlands, 2000. ISBN 9058083136.143 p.
51. Krishnan JM, Deshpande AP, Kumar PS, editors. Rheology of complex fluids. New York: Springer; 2010. p. 3–34.
52. Orliac O, Silvestre F, Rouilly A, Rigal L. Rheological studies, production, and characterization of injection-molded plastics from sunflower protein isolate. Ind Eng Chem Res. 2003;42(8):1674.
53. Ancey C. Plasticity and geophysical flows: a review. J Nonnewton Fluid Mech. 2007;142(1–3):4.
54. White CC, VanLandingham MR, Drzal PL, Chang NK, Chang SH. Viscoelastic characterization of polymers using instrumented indentation. II. Dynamic testing. J Polym Sci B: Polym Phys. 2005;43(14):1812–24.
55. Junior FE, Macedo FC, Farias MM. A methodology to assess the evolution of viscoelastic properties of hardened cement pastes through dynamic mechanical analysis. Constr Build Mater. 2019;226:849.
56. Bengoechea C, Cordobés F, Guerrero A. Rheology and microstructure of gluten and soya-based o/w emulsions. Rheol Acta. 2006;46:13.
57. Isnaini L, Estiasih T, Suseno SH, Lestari LA. The role vegetable proteins to stabilize emulsion: A mini review. IOP Conf Ser: Earth Environ Sci. 2021;924(1):012036). IOP Publishing.
58. Meirelles AAD, Costa ALR, Cunha RL. Cellulose nanocrystals from ultrasound process stabilizing O/W Pickering emulsion. Int J Biol Macromol. 2020;158:75–84.
59. Cerimedo MSÁ, Iriart CH, Candal RJ, Herrera ML. Stability of emulsions formulated with high concentrations of sodium caseinate and trehalose. Food Res Int. 2010;43(5):1482–93.
60. Mcclements DJ. Critical review of techniques and methodologies for characterization of emulsion stability. Crit Rev Food Sci Nutr. 2007;47(7):611–49.
61. Niu H, Wang W, Dou Z, Chen X, Chen X, Chen H, Fu X. Multiscale combined techniques for evaluating emulsion stability: a critical review. Adv Coll Interface Sci. 2023;311:102813.
62. Rosso A, Lollo G, Chevalier Y, Troung N, Bordes C, Bourgeois S, et al. Development and structural characterization of a novel nanoemulsion for oral drug delivery. Colloids Surf A: Physicochem Eng Aspect. 2020;593:124614. https://doi.org/10.1016/j.colsurfa.2020.124614.
63. Schreiner TB, Santamaria-Echart A, Ribeiro A, Peres AM, Dias MM, Pinho SP, et al. Formulation and optimization of nanoemulsions using the natural surfactant saponin from Quillaja bark. Molecules (Basel, Switzerland). 2020;25(7):1538. https://doi.org/10.3390/molecules25071538.
64. McClements DJ. Protein-stabilized emulsions. Curr Opin Colloid Interface Sci. 2004;9(5):305–13.
65. Abedi Karjiban R, Fard Masoumi HR, Basri M, Abdul Malek E, Samson S. Design and development of a nanoemulsion system containing copper peptide by D-optimal mixture design and evaluation of its physicochemical properties. RSC Adv. 2016;6(22):17845–56.